

## Monitoring the required energy for the crack propagation of fiber-reinforced cementitious composite

Sajjad Mirzamohammadi<sup>1a</sup> and Moosa Mazloom<sup>\*2</sup>

<sup>1</sup> Department of structural Engineering, Tarbiat Modares University, Tehran, Iran

<sup>2</sup> Department of Civil Engineering, Shahid Rajaee Teacher Training University, Tehran, Iran

(Receive July 30, 2021, Revised August 25, 2021, Accepted September 1, 2021)

**Abstract.** In this paper, the results of experimental work on the required energy for the crack propagation (fracture energy), rupture modulus and compressive strength of fiber-reinforced cementitious composite (FRCC) with different types of fibers after exposure to 20°C, 100°C and 300°C are investigated. The experimental part of the work is divided into the following stages: the effects of sub-elevated temperatures and fiber types on the fracture and mechanical behaviors of FRCC; finding a relation between the fracture energy and mechanical properties of the specimens based on I-optimal design of response surface methodology (RSM-I-optimal). Specifically, the analysis of variance (ANOVA) was examined to evaluate the influences of compressive strength and rupture modulus on the required energy for the crack propagation. For this purpose, three monotype fiber reinforced mixes have been prepared. The utilized fibers were aramid, basalt and glass. Additionally, the predictive efficiency of the RSM model was studied based on the normalized goodness-of-fit statistics (Nash & Sutcliffe coefficient of efficiency, *NSE*). The main finding was that both compressive strength and rupture modulus had considerable influences on the fracture energy. However, the effect of rupture modulus was far greater than compressive strength. In terms of *NSE* value, the model predictive efficiency was good for fracture energy.

**Keywords:** monotype fibers; analysis of variance; rupture modulus; crack propagation; fracture energy

### 1. Introduction

The acceptable compressive strength of concrete is a sign that makes it reliable in the construction industry (Mazloom 2008). Nevertheless, the big weakness point of concrete is its tensile strength, which creates brittle fractures when exposed to tensile stresses (Mazloom and Mirzamohammadi 2021a). This trouble is the main reason for presenting fibers into the world of concrete. The purpose of adding fibers to concrete mix proportions are: greater ductility, superior energy absorption, durability development, crack reduction and tensile strength improvement. Moreover, improving the rupture modulus of concrete is its most important specification (Yang and Li 2010, Mo *et al.* 2018, Zhang *et al.* 2019, Mazloom and Mirzamohammadi 2019). The progress of fiber reinforced concrete (FRC) has experienced many variations, and fiber-reinforced cementitious composite (FRCC) forms a specific category in FRC, which its main ingredients are

---

\*Corresponding author, Professor, E-mail: mazloom@sru.ac.ir; moospoon@yahoo.com

<sup>a</sup> Ph.D., E-mail: Sajadmirzamohammadi@gmail.com

water, cement, fiber and fine aggregate. It should be emphasized that many studies have been carried out on revising the components of FRCC, such as modifying the type of fibers and changing cement matrix components (Sahmaran and Li 2007, Li 2008, Şahmaran *et al.* 2010, 2011, Yu *et al.* 2014, 2015).

The required energy for the crack propagation or fracture energy of concrete and FRCC is an important item for studying its crack propagation. Some researchers have studied the fracture behavior of different kinds of concrete, including FRCC, self-compacting normal, and lightweight concrete (Nikbin *et al.* 2016, Karamloo *et al.* 2016, 2017, Karamloo and Mazloom 2018, Salehi and Mazloom 2018, 2019a, b). Fracture parameters like fracture toughness ( $K_{IC}$ ), fracture energy ( $G_f$ ), critical effective crack-tip opening displacement ( $\delta_c$ ) and the length of fracture process zone ( $C_f$ ) are important to estimate the effects of cracking on the elements. According to Wang *et al.* (2016), provided that the elastic energy stored in a zone of concrete becomes higher than its fracture energy, it leads to the formation of micro-cracks in the specimen. These micro-cracks may cause macroscopic fractures. Consequently, the crack growth in concrete can lead to decreasing the durability and serviceability of the structure.

Response surface methodology (RSM) is a suitable statistical and mathematical tool for studying the relationship between the effects of some discrete parameters influencing the responses by varying these parameters simultaneously. Alternatively stated, it studies the relationship between the independent parameters (factors) and the responses of the problems (Mohammed *et al.* 2018, Şimşek *et al.* 2018, Tyagi *et al.* 2018, Mazloom and Mirzamohammadi 2021b). I-optimal design (RSM-I-optimal) is one of the most common procedures used under RSM for empirical modeling. Therefore, the response model based on I-optimal is illustrated in Eq. (1) (Awolusi *et al.* 2019).

$$Y = (b_0 + \varepsilon) + \sum_{i=1}^k b_i X_i + \sum_{i=1}^k b_{ii} X_i^2 + \sum_{i=1}^k \sum_{j=i+1}^k b_{ij} X_i X_j \quad (1)$$

Where  $Y$  and  $k$  denote response values and number of factors.  $b_0$ ,  $b_i$ ,  $b_{ii}$  and  $b_{ij}$  coefficients are determined by the least-squares method,  $X_i$  and  $X_j$  ( $i \neq j$ ) factors are independent parameters and  $\varepsilon$  is errors.

Some studies have been conducted on different kinds of concrete to discovery suitable equations by RSM. Awolusi *et al.* (2019) detected several relationships to estimate slump, water absorption, compressive, flexural and splitting tensile strengths of concrete reinforced with steel fibers. The models were in terms of (independent parameters) fiber aspect ratio, water to cement ratio, and cement. Alsanusi and Bentaher (2015) discovered some relations to predict the compressive strength of ordinary concrete at the age of 28 days. Independent parameters were mix components and the concrete compressive strength of the age of 7 days. Some researchers used RSM method to optimize the mix proportions of concrete (Murray *et al.* 2014, Jimma and Rangaraju 2015, Al-alaily and Hassan 2016, Rezaifar *et al.* 2016). Although various investigators have tried to discover some equations to predict concrete and FRCC mechanical properties (Mazloom and Ranjbar 2010, Mazloom and Yoosefi 2013, Mazloom *et al.* 2019), only few researches have revealed some equations based on RSM (the I-optimal) to predict fracture energy.

Despite many advantages of fiber reinforced concrete (FRC) and fiber-reinforced cementitious composite (FRCC), their behavior after exposure to high or elevated temperature presents a major concern for researchers. When exposed to higher temperatures, a reinforced cementitious material may be subjected to a high or low degree of damage. Heating causes different changes in its

properties and, in particular, changes in the microstructure accompanied by the loss of mechanical strength. Since the benefits of application of fibers on concrete mechanical, fracture, and durability properties have been proven, the present study is conducted to evaluate fracture energy, rupture modulus and compressive strength after exposure to normal and elevated temperatures (20°C, 100°C and 300°C). Furthermore, this study investigates a relation to predict the fracture energy based on the new method (RSM).

In this study, the experimental part of the work has three phases. First, the effects of fiber types on the compressive strength, rupture modulus and fracture energy of FRCC are studied. Secondly, the effects of sub-elevated temperatures on the mentioned parameters with different types of fibers are investigated. Eventually, a model is developed between the response (fracture energy) and independent parameters (Compressive strength and rupture modulus).

## 2. Experimental program

### 2.1 Materials and specimen preparation

Table 1 shows the details of the mixtures for all fiber types. The cementitious materials used for mix proportions were ordinary Portland cement (OPC) and silica fume (SF). It must be noted that silica fume is a tremendously reactive cementitious material, and it can develop the creation of secondary hydration products (Mazloom and Miri 2017, Mazloom *et al.* 2017, 2018a, b, Afzali Naniz and Mazloom 2018, 2019a, b). The chemical compositions of the cementitious materials can be seen in Table 2. The silica sand used as the aggregate in this study had the minimum and maximum grain sizes of 130  $\mu\text{m}$  and 250  $\mu\text{m}$ , respectively. To attain the wanted rheology of cement mortars, a polycarboxylate-based high-range water reducing admixture (HRWRA) was used in the mixes. For establishing equal circumstances, the values of aramid, basalt, and glass fibers were 2% volume. Table 3 indicates the geometrical and mechanical properties of the fibers.

It is noteworthy that in the first step, silica sand and fibers were moved to the mixer and mixed for 5 minutes. Then, the silica fume and cement contents were added, respectively; afterwards, they were mixed for 1 minute. Lastly, water and HRWRA were added and mixed for 3 minutes. The fresh cement mortars were poured into the molds and protected with plastic sheets. After one day, the samples were demolded and cured for 27 days. Except for the temperature of 20°C, all the samples were warmed in a furnace to the temperatures of 100°C and 300°C for one hour, and the heating rate was 10°C/min. Then, the specimens were exposed to the room temperature and cooled

Table 1 Mix proportions of FRCC

|  |       |
|--|-------|
| Cement ( $\text{kg}/\text{m}^3$ )      | 850   |
| Silica fume ( $\text{kg}/\text{m}^3$ ) | 160   |
| Silica sand ( $\text{kg}/\text{m}^3$ ) | 588   |
| Water ( $\text{kg}/\text{m}^3$ )       | 390   |
| HRWRA ( $\text{kg}/\text{m}^3$ )       | 16    |
| Fiber*                                 | 2%vol |
| W/(C+SF)                               | 0.38  |

\*Aramid, Basalt, and Glass

Table 2 Chemical composition of cement and SF

|  | OPC   | SF   |
|--|-------|------|
| Silicon dioxide (SiO <sub>2</sub> ): wt%                   | 21.30 | 96.4 |
| Calcium oxide (CaO): wt%                                   | 63.48 | 0.49 |
| Aluminium oxide (Al <sub>2</sub> O <sub>3</sub> ): wt%     | 5.13  | 1.32 |
| Ferric oxide (Fe <sub>2</sub> O <sub>3</sub> ): wt%        | 3.47  | 0.87 |
| Sodium oxide (Na <sub>2</sub> O): wt%                      | 0.23  | 0.31 |
| Magnesium oxide (MgO): wt%                                 | 2.51  | 0.97 |
| Phosphorus pentoxide (P <sub>2</sub> O <sub>5</sub> ): wt% | -     | 0.16 |
| Sulfur trioxide (SO <sub>3</sub> ): wt%                    | 1.67  | 0.10 |
| Potassium oxide (K <sub>2</sub> O): wt%                    | 0.56  | 1.01 |
| Silicon carbide (SiC): wt%                                 | -     | 0.5  |
| Carbon (C): wt%  | -     | 0.3  |
| Chloride (CL): wt%   | -     | 0.04 |
| Water (H <sub>2</sub> O): wt%                              | -     | 0.08 |

Table 3 Properties of fibers

| Fiber type | Diameter, $\mu\text{m}$ | Length, mm | Tensile strength, MPa | Young modulus, GPa | Density, Kg/m <sup>3</sup> | Melting Point, °C |
|------------|-------------------------|------------|-----------------------|--------------------|----------------------------|-------------------|
| Aramid     | 12                      | 10         | 3150                  | 80                 | 1440                       | 800               |
| Basalt     | 11                      | 10         | 2950                  | 90                 | 2670                       | 600               |
| Glass      | 20                      | 10         | 3450                  | 69                 | 2550                       | 1400              |

Table 4 Specimen numbers for each mix proportion

| Temperature, °C | Compressive strength test | Four-point bending test |
|-----------------|---------------------------|-------------------------|
| 20              | 3                         | 3                       |
| 100             | 3                         | 3                       |
| 300             | 3                         | 3                       |

naturally. Table 4 shows the number of the samples. Figs. 1 and 2 illustrate the mixing and test procedures.

## 2.2 Methodology

RSM is normally used under circumstances where numerous features affect one or more performance responses or characteristics. In other words, RSM opens new opportunities in the categorization and generality of available empirical results for assessing FRCC strengths. The application of I-optimal with RSM includes four main steps.

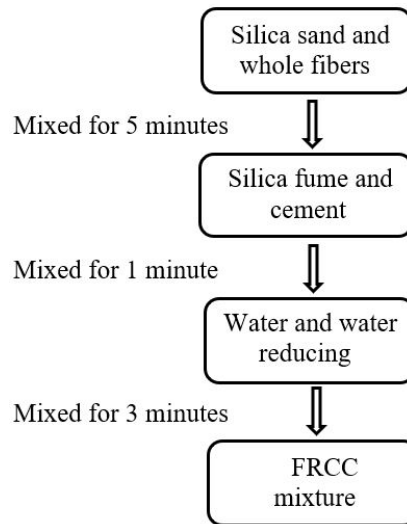


Fig. 1 Mix process

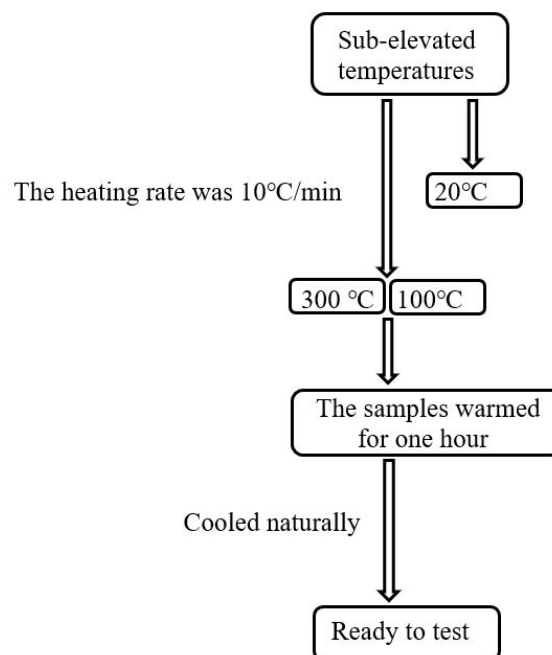


Fig. 2 Test process

- 1) Providing an experimental design according to the selected settings.
- 2) Running experiments with statistical design.
- 3) Estimating the coefficients in the mathematical model and checking the model accuracy.
- 4) Performing response analysis for prediction of optimum settings, which are proven through experimentation. In this research, the RSM (I-optimal design) was designated to determine the

relationship between two factors and response. The factors with code levels are illustrated in Table 5. likewise, the predictive efficiency of the RSM model was studied based on the normalized goodness-of-fit statistics (Nash & Sutcliffe coefficient of efficiency, *NSE*) as defined in Eqs. (2) to (6) (Ritter and Muñoz-Carpena 2013).

$$NSE = 1 - \left(\frac{RMSE}{SD}\right)^2 \quad \text{or} \quad NSE = 1 - \left(\frac{1}{n_t + 1}\right)^2 \quad (2)$$

$$RMSE = (MSE)^{\frac{1}{2}} \quad (3)$$

$$MSE = \frac{\sum_{i=1}^n (Y_i - O_i)^2}{n} \quad (4)$$

$$SD = \left(\frac{\sum_{i=1}^n (O_i - \bar{o})^2}{n}\right)^{\frac{1}{2}} \quad (5)$$

Table 5 Independent parameters with code levels

| Factor (Symbol) | Independent variables (factors) | Units | Code levels |    |
|-----------------|---------------------------------|-------|-------------|----|
|                 |                                 |       | -1          | +1 |
| A               | Compressive strength            | MPa   | 43          | 75 |
| B               | Rupture modulus                 | MPa   | 4           | 10 |

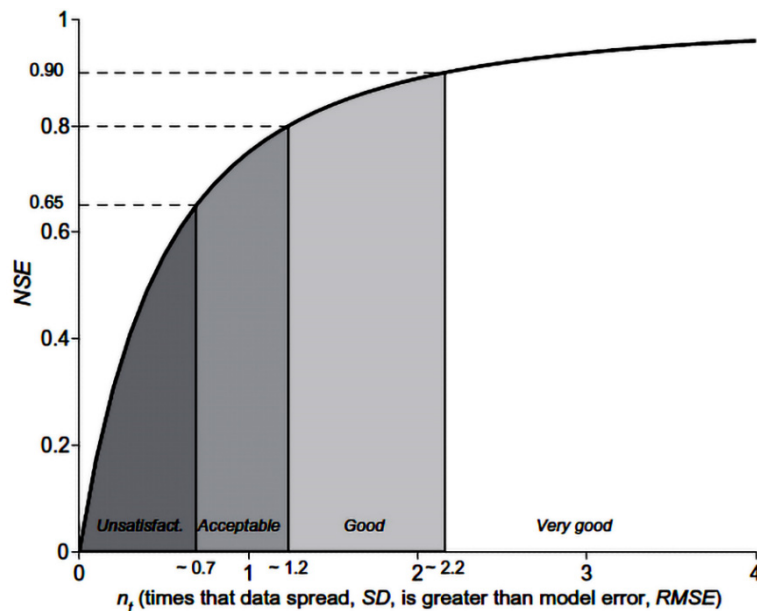


Fig. 3 Relationship between *NSE* and model mean error relative to the spread of the observations (Ritter and Muñoz-Carpena 2013)

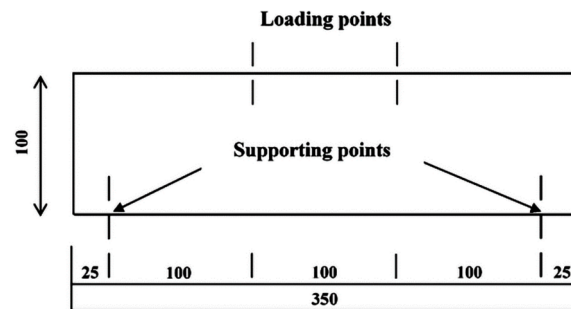


Fig. 4 Arrangement for the rupture modulus test

$$n_t = \frac{SD}{RMSE} - 1 \quad (6)$$

where  $MSE$ ,  $RMSE$  and  $SD$  are mean square error, root-mean-square error and standard deviation, respectively. Moreover,  $Y_i$ ,  $O_i$ ,  $\bar{o}$  and  $n$  are predicted, experimental, mean of the experimental and number of values, respectively. In terms of  $NSE$ , the model performance rating is classified unsatisfactory, acceptable, good and very good as illustrated in Fig. 3 (Ritter and Muñoz-Carpena 2013).

### 3. Test set up and procedures

#### 3.1 Compressive strength test

To specify the compressive strength of the specimens, ADR Touch machine built in UK was used. The specimens were  $15 \times 15 \times 15 \text{ cm}^3$  cubes according to BS 1881: part 111: 1983 (BSI 1983). Furthermore, the loading speed was equal to 0.3 MPa/s.

#### 3.2 Four-point-bending test (Rupture modulus)

Fig. 4 illustrates the preparation of the rupture modulus test, which is according to ASTM C1609 (ASTM C1609/M-05 2006). The preferred dimensions of the beams are  $150 \times 150 \times 750 \text{ mm}^3$ . However, if the maximum size of aggregate is less than 25 mm,  $100 \times 100 \times 500 \text{ mm}^3$  beams may be used. In this study, tests were done on the samples with the dimensions of  $100 \times 100 \times 350 \text{ mm}^3$ . The machine used to explore the rupture modulus of the specimens was Zwick Roell built in Germany. Additionally, the loading rate was 0.5 mm/min.

## 4. Result and discussion

### 4.1 Compressive strength

Fig. 5 depicts the compressive strength of the specimens at three temperatures of 20°C, 100°C, and 300°C respectively. The maximum compressive strength at all temperatures was related to the specimens containing aramid fibers. Furthermore, the minimum average compressive strength was

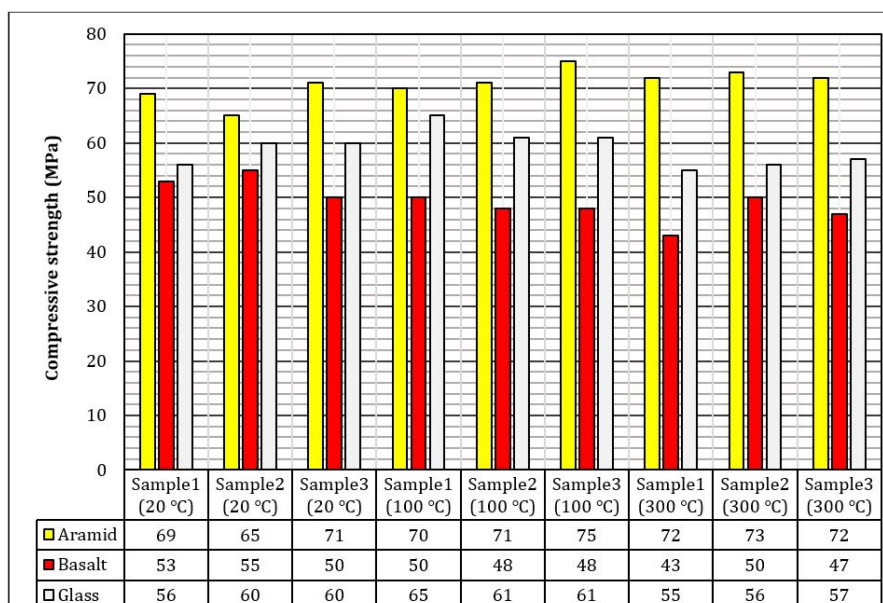


Fig. 5 Compressive strength of the specimens

related to the specimens containing basalt fibers after the exposure to 20°C, 100°C and 300°C. According to Fig. 5, the compressive strength of the samples having aramid fibers improved by 4.5% and 5% at 100°C and 300°C respectively. It may be because of the strengthened cement paste during the evaporation of free water. Actually, the cement gel layers relocated nearer to each other at higher temperatures and prepared superior Van der Waal's forces (Dias *et al.* 1990, Khoury 1992). Moreover, the hydration of cement particles that have not contributed in the hydration process in lower temperatures can be mentioned (Morsy *et al.* 2012). Finally, the average compressive strength of the specimens having glass fibers enhanced by 6% at 100°C and diminished by 5% after exposure to 300°C. In other words, sub-elevated temperatures did not have significant effects on the compressive strength of the samples and some studies are in agreement with the mentioned results (Morsy *et al.* 2012).

#### 4.2 Rupture modulus

Fig. 6 shows the rupture modulus of the samples after exposure to 20°C, 100°C, and 300°C respectively. As is obvious in this figure, the greatest average rupture modulus was related to the specimens having glass fibers at normal temperature (20°C). Nevertheless, at elevated temperatures (300°C), the maximum average rupture modulus was related to the specimens having aramid fibers in most situations. In addition, the average rupture modulus of all the specimens decreased by increasing the temperature. It means, using glass fibers with the greatest melting points could not increase the rupture modulus of the specimens at elevated temperatures. Microstructures of the specimens at mentioned temperatures were examined using scanning electron microscopy (SEM). The SEM images revealed that the structure of samples were homogeneous and compressed (Figs. 7(a) and (b)). Also, a few air pores and cracks were detected in the specimens, which was the main reason for decreased rupture modulus of samples (Figs. 7(c),

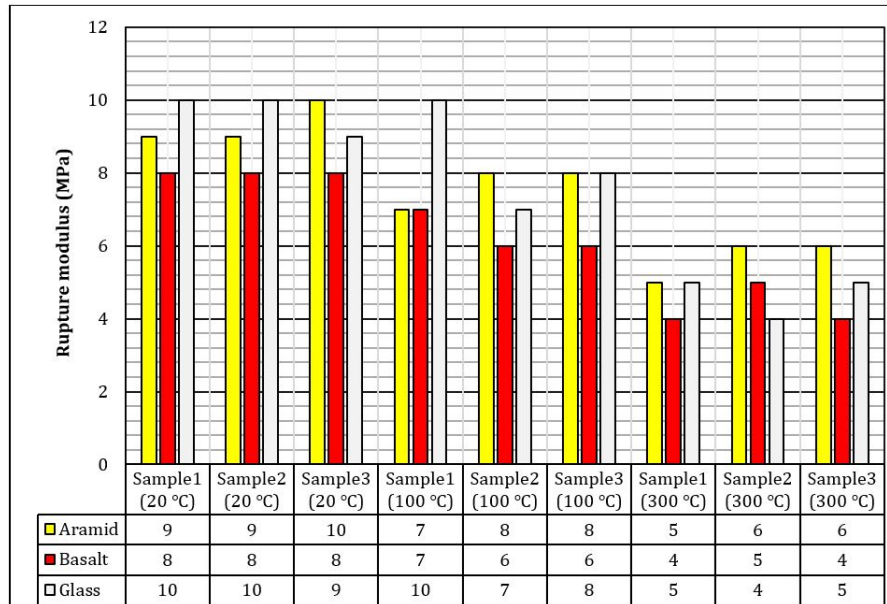


Fig. 6 Rupture modulus of the samples

(d) and (e)). In other words, a temperature rise can reduce the van der waal's forces between C-S-H layers and create silanol groups (Si-OH), leading to an increased number of micro-cracks.

#### 4.3 The required energy for the crack propagation (Fracture energy)

For calculating the fracture energies of the specimens, the recommendations of RILEM Committee 50-FMC were used (RILEM Committee 50-FMC). It should be noted that the fracture energy ( $G_F$ ) of the specimens can be defined as the total area under the load-deflection curve ( $W$ ) divided by its broken cross section ( $a$ ) (Hillerborg 1985). In other words, fracture energy can be calculated by the following equations

$$G_F = \frac{W}{a} \quad (7)$$

$$W = W_0 + W_1 + W_2 \quad (8)$$

$$W_1 = W_2 = F_1 \delta_0 \quad (9)$$

The deformation when the beam breaks is  $\delta_0$  and  $F_1$  is the weight of testing equipment and the beam.

Fig. 8 represents the fracture energies of the samples presented above. Note that these values are for average load-deformation curves at elevated temperatures. According to this Fig, using glass fibers with the maximum melting point could increase the fracture energy of the specimens at 100°C; however, it was not successful at 300°C. In other words, the melting point of fibers did not have significant positive effect on the fracture energy of the specimens at elevated temperatures. Moreover, this Fig shows that the average fracture energies of the samples with

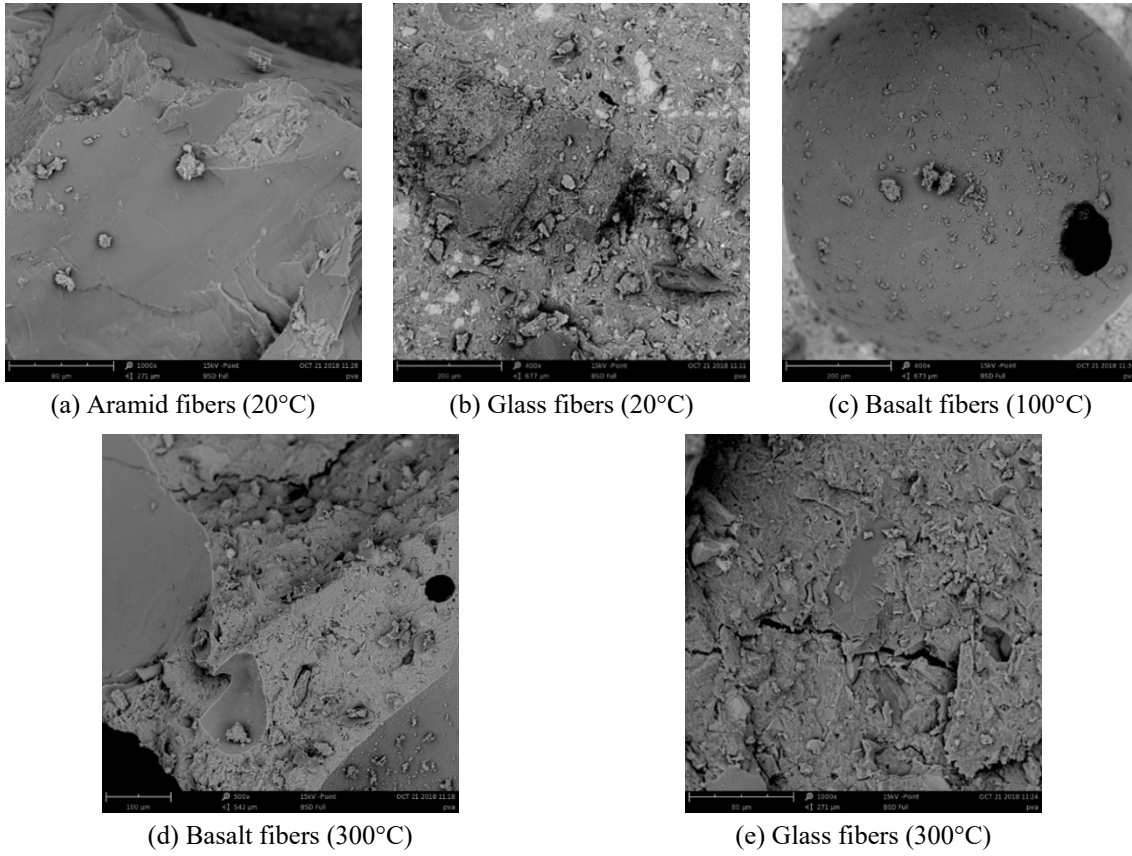


Fig. 7 Microstructure of the specimens

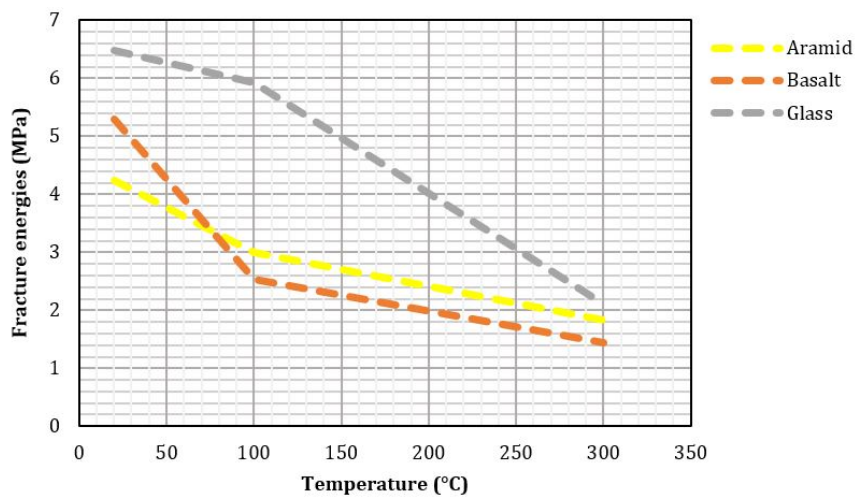


Fig. 8 Fracture energies of the specimens

aramid, basalt and glass fibers dropped by 30%, 52.5% and 8.5% at 100°C, respectively. Furthermore, the average fracture energy of the specimens reinforced with aramid, basalt and glass fibers declined by 57%, 73% and 68% at 300°C, respectively. It means, the negative effect of sub-elevated temperatures on fracture energy was much more than its drawback on the rupture modulus.

Eq. (10) shows the relation between fracture energy ( $G_F$ ) and independent parameters, which are achieved by The RSM (I-optimal design) in terms of experimental factors. Fig. 9 indicates the analysis of variance (ANOVA) for response. It is clear that both compressive strength and rupture modulus have a notable effect on the fracture energy ( $p$ -value  $< 0.05$ ). P-Values larger than 0.1000 denote the model terms are not important. In other words,  $B^2$  ( $p$ -value  $> 0.1$ ) is not significant in this model. It is worth mentioning that the impacts of rupture modulus on the fracture energy are far greater than compressive strength. Moreover, Eq. (11) represents the final equation in terms of coded factors. According to this equation, the effect of rupture modulus on fracture energy was positive (+ 2.41B). In other words, increase occurred in the fracture energy of samples when the rupture modulus increased. Fig. 10 depicts the cracks of the samples under compressive strength and four-point bending tests.

$$\text{Fracture energy} = -20.58704 + 0637941A + 1.22470B - 0.021559AB - 0.004539A^2 + 0.060649B^2 \quad (10)$$

$$\text{Fracture energy} = +3.89 - 0.7767A + 2.41B - 1.3AB - 1.16A^2 + 0.5458B^2 \quad (11)$$

#### 4.4 Predictive efficiency of the RSM model

Numerous methods for calculating the goodness-of-fit of observations against model-calculated values have been proposed but none of them is free of limitations and are often ambiguous. The

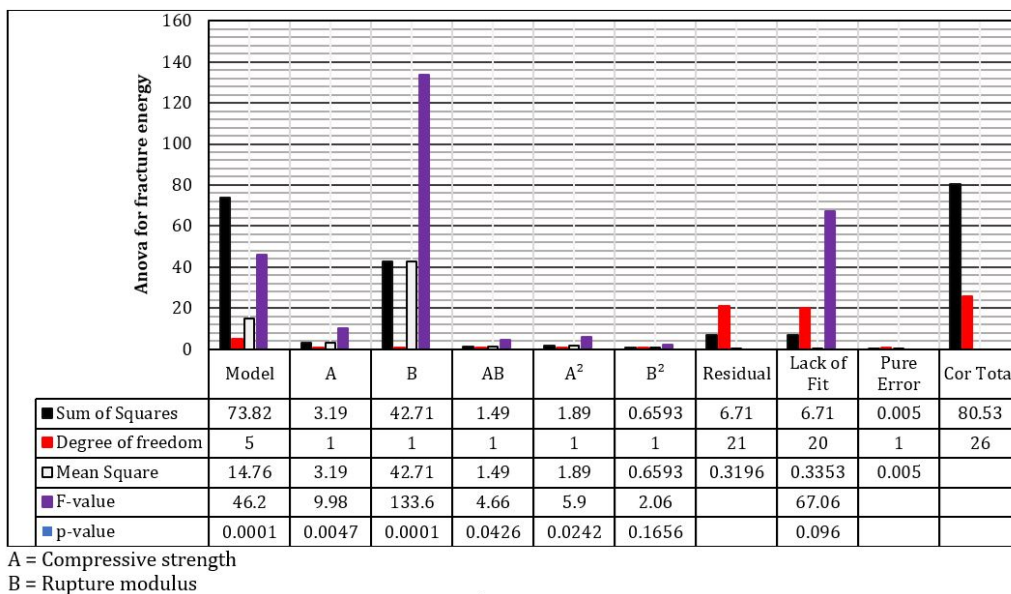


Fig. 9 Analysis of variance for fracture energy

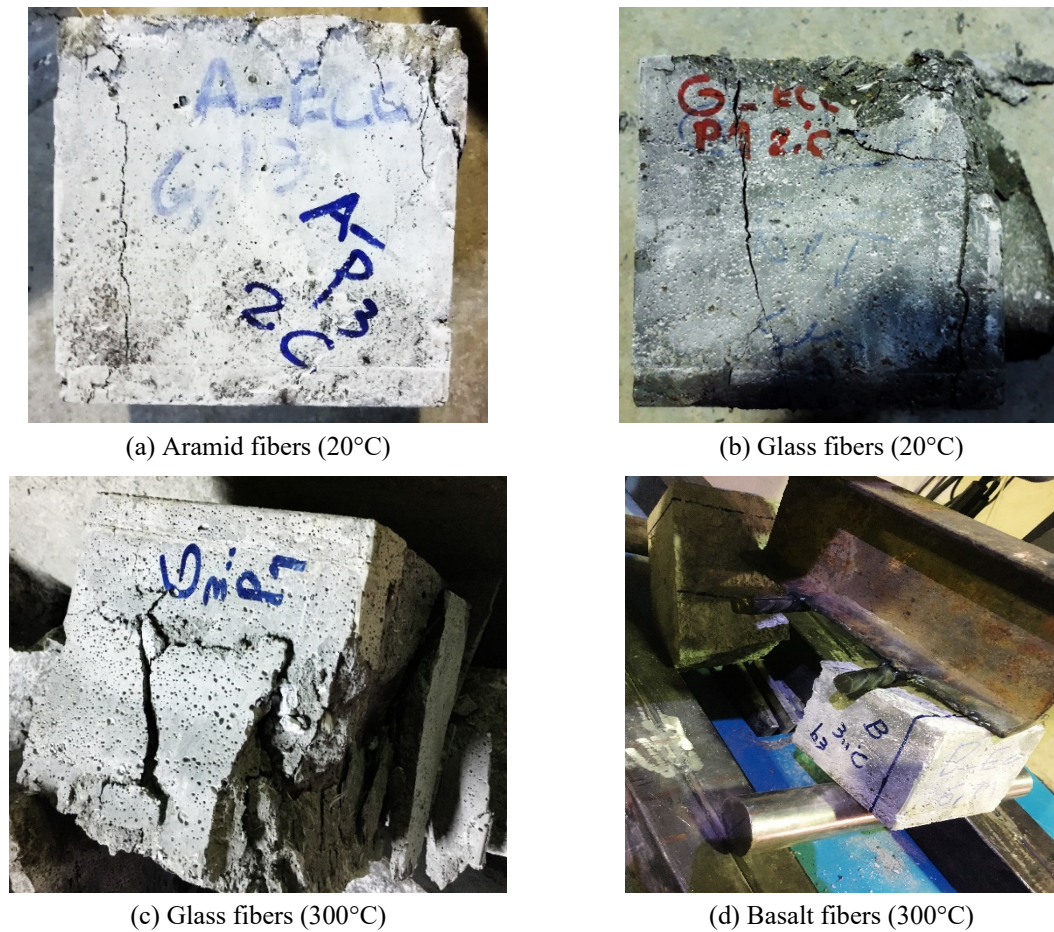


Fig. 10 Cracks of the samples under compressive strength and four-point bending tests

Table 6 Predictive efficiency of the RSM model

| Test                       | <i>SD</i> | <i>MSE</i> | <i>RMSE</i> | $n_t$ | <i>NSE</i> | Model classification |
|----------------------------|-----------|------------|-------------|-------|------------|----------------------|
| Fracture energy (Eq. (10)) | 1.78      | 0.45       | 0.67        | 1.62  | 0.85       | good                 |

Nash & Sutcliffe coefficient of efficiency (*NSE*) is a widely used indicator due to its flexibility to be applied to various types of mathematical models like RSM. This research assesses the predictive efficiency of the RSM model between experimental and predicted values based on *NSE* method (Ritter and Muñoz-Carpena 2013). Standard deviation (*SD*), mean square error (*MSE*), root-mean-square error (*RMSE*), Nash & Sutcliffe coefficient of efficiency (*NSE*), and model classification are described in Table 6. In terms of *NSE*, the model performance rating is classified unsatisfactory, acceptable, good and very good when  $NSE < 0.65$ ,  $0.65 \leq NSE < 0.8$ ,  $0.8 \leq NSE < 0.9$  and  $NSE \geq 0.9$ , respectively. According to this table, the model classification is good for fracture energy. Awolusi *et al.* (2019) discovered some relations to predict slump, water absorption, compressive strength, flexural strength and splitting tensile strength of concrete

reinforced with steel fibers. The model classification was very good for slump, water absorption, compressive strength and splitting tensile strength, but it was acceptable for flexural strength. It should be noted that independent parameters were fiber aspect ratio, water to cement ratio and cement.

## 5. Conclusions

From the results of this research, the following conclusions can be derived:

- According to the results of experimental work, using glass fibers with the maximum melting point could increase the required energy for the crack propagation of the specimens at 100°C; however, it was not successful at 300°C. In other words, the melting point of fibers did not have significant positive effect on the fracture energy of the specimens at elevated temperatures.
- The detrimental effect of sub-elevated temperatures on the required energy for crack propagation was much more than its drawback in rupture modulus. In fact, the required energy for the crack propagation of the samples decreased about 30% and 66% on average at 100°C and 300°C, respectively. In fact, a temperature rise can diminish the van der waal's forces between C-S-H layers and create silanol groups (Si-OH), leading to an increased number of micro-cracks.
- RSM model predictive efficiency was good for fracture energy.
- The analysis of variance (ANOVA) for fracture energy expressed that both compressive strength and rupture modulus had considerable influences on the fracture energy. However, the effect of rupture modulus was far greater than compressive strength.
- Rupture modulus had considerable positive impact on the required energy for the crack propagation of the samples. It means the fracture energy of all the specimens improved by increasing the rupture modulus. Additionally, the effect of compressive strength was not considerable on the fracture energy of some samples. The highest fracture energy was related to the specimens having the most rupture modulus values.

## References

- Afzali-Naniz, O. and Mazloom, M. (2018), "Effects of colloidal nano-silica on fresh and hardened properties of self-compacting lightweight concrete", *J. Build. Eng.*, **20**, 400-410.  
<https://doi.org/10.1016/j.jobe.2018.08.014>
- Afzali-Naniz, O. and Mazloom, M. (2019a), "Assessment of the influence of micro- and nano-silica on the behavior of self-compacting lightweight concrete using full factorial design", *Asian J. Civil Eng.*, **20**, 57-70. <https://doi.org/10.1007/s42107-018-0088-2>
- Afzali-Naniz, O. and Mazloom, M. (2019b), "Fracture behavior of self-compacting semi-lightweight concrete containing nano-silica", *Adv. Struct. Eng.*, **22**(10), 2264-2277.  
[https://doi: 10.1177/1369433219837426](https://doi:10.1177/1369433219837426)
- Al-alaily, H.S. and Hassan, A.A. (2016), "Refined statistical modeling for chloride permeability and strength of concrete containing metakaolin", *Constr. Build. Mater.*, **114**, 564-579.  
<https://doi.org/10.1016/j.conbuildmat.2016.03.187>
- Alsansu, S. and Bentaher, L. (2015), "Prediction of compressive strength of concrete from early age test result using design of experiments (RSM)", *Int. J. Civil Environ. Struct. Constr. Archit. Eng.*, **9**(12), 1559-

1563.

- ASTM C1609/M-05 (2006), Standard Test Method for Flexural Performance of Fiber Reinforced Concrete (using Beam with Third-point loading), ASTM International, West Conshohocken, PA, USA.
- Awolusi, T.F., Oke, O.L., Akinkulore, O.O. and Sojobi, A.O. (2019), "Application of response surface methodology: Predicting and optimizing the properties of concrete containing steel fiber extracted from waste tires with limestone powder as filler", *Case Studies Constr. Mater.*, **10**, e00212. <https://doi.org/10.1016/j.cscm.2018.e00212>
- BSI 1881: part 111. (1983), Method of testing concrete, British Standards.
- Dias, W.P.S., Khoury, G.A, and Sullivan, P.J.E. (1990), "Mechanical properties of hardened cement paste exposed to temperatures up to 700°C (1292°F)", *ACI Mater.*, **87**, 160-166.
- Hillerborg, A. (1985), "The theoretical basis of a method to determine the fracture energy  $G_f$  of concrete", *Mater. Struct.*, **18**(4), 291-296. <https://doi.org/10.1007/BF02472919>
- Jimma, B.E. and Rangaraju, P.R. (2015), "Chemical admixtures dose optimization in pervious concrete paste selection—A statistical approach", *Constr. Build. Mater.*, **101**, 1047-1058. <https://doi.org/10.1016/j.conbuildmat.2015.10.003>
- Karamloo, M. and Mazloom, M. (2018), "An efficient algorithm for scaling problem of notched beam specimens with various notch to depth ratios", *Comput. Concrete, Int. J.*, **22**(1), 39-51. <http://dx.doi.org/10.12989/cac.2018.22.1.039>
- Karamloo, M., Mazloom, M. and Payganeh, G. (2016), "Effects of maximum aggregate size on fracture behaviors of self-compacting lightweight concrete", *Constr. Build. Mater.*, **123**, 508-515. <https://doi.org/10.1016/j.conbuildmat.2016.07.061>
- Karamloo, M., Mazloom, M. and Payganeh, G. (2017), "Effect of size on nominal strength of self-compacting lightweight concrete and self-compacting normal weight concrete: A stress-based approach", *Mater. Today Commun.*, **13**, 36-45. <https://doi.org/10.1016/j.mtcomm.2017.08.002>
- Khoury, G.A. (1992), "Compressive strength of concrete at high temperatures: a reassessment", *Mag. Concrete Res.*, **161**, 291-309. <https://doi.org/10.1680/mac.1992.44.161.291>
- Li, V.C. (2008), "Durability of mechanically loaded engineered cementitious composites under highly alkaline environments", **30**, 72-81. <https://doi.org/10.1016/j.cemconcomp.2007.09.004>
- Mazloom, M. (2008), "Estimating long-term creep and shrinkage of high-strength concrete", *Cem. Concrete Compos.*, **30**(4), 316-326. <https://doi.org/10.1016/j.cemconcomp.2007.09.006>
- Mazloom, M. and Miri, M.S. (2017), "Interaction of magnetic water, silica fume and superplasticizer on fresh and hardened properties of concrete", *Adv. Concrete Constr., Int. J.*, **5**(2), 87-99. <https://doi.org/10.12989/acc.2017.5.2.087>
- Mazloom, M. and Mirzamohammadi, S. (2019), "Thermal effects on the mechanical properties of cement mortars reinforced with aramid, glass, basalt and polypropylene fibers", *Adv. Mater. Res., Int. J.*, **8**(2), 137-154. <http://dx.doi.org/10.12989/amr.2019.8.2.137>
- Mazloom, M. and Mirzamohammadi, S. (2021a), "Fracture of fibre-reinforced cementitious composites after exposure to elevated temperatures", *Mag. Concrete Res.*, **73**(14), 701-713. <https://doi.org/10.1680/jmacr.19.00401>
- Mazloom, M. and Mirzamohammadi, S. (2021b), "Computing the fracture energy of fiber reinforced cementitious composites using response surface methodology", *Adv. Comput. Des., Int. J.*, **6**(3), 225-239. <http://dx.doi.org/10.12989/acd.2021.6.3.225>
- Mazloom, M. and Ranjbar, A. (2010), "Relation between the workability and strength of self-compacting concrete", *Proceedings of the 35th Conference on Our World in Concrete & Structures*, Singapore, pp. 315-322.
- Mazloom, M. and Yoosefi, M.M. (2013), "Predicting the Indirect Tensile Strength of Self Compacting Concrete Using Artificial Neural Networks", *Comput. Concrete, Int. J.*, **12**(3), 285-301. <https://doi.org/10.12989/cac.2013.12.3.285>
- Mazloom, M., Allahabadi, A. and Karamloo, M. (2017), "Effect of silica fume and polyepoxide-based polymer on electrical resistivity", *Adv. Concrete Constr., Int. J.*, **5**(6), 587-611. <https://doi.org/10.12989/acc.2017.5.6.587>

- Mazloom, M., Homayooni, S.M. and Miri, S.M. (2018a), "Effect of rock flour type on rheology and strength of self-compacting lightweight concrete", *Comput. Concrete, Int. J.*, **21**(2), 199-207. <https://doi.org/10.12989/cac.2018.21.2.199>
- Mazloom, M., Soltani, A., Karamloo, M., Hasanloo, A. and Ranjbar, A. (2018b), "Effects of silica fume, superplasticizer dosage and type of superplasticizer on the properties of normal and self-compacting concrete", *Adv. Mater. Res., Int. J.*, **7**(1), 407-434. <https://doi.org/10.12989/amr.2018.7.1.045>
- Mazloom, M., Pourhaji, P., Shahveisi, M. and Jafari, S.H. (2019), "Studying the Park-Ang damage index of reinforced concrete structures based on equivalent sinusoidal waves", *Struct. Eng. Mech., Int. J.*, **72**(1), 845-859. <https://doi.org/10.12989/sem.2019.72.1.083>
- Mo, K.H., Loh, Z.P. and Tan, C.G., Alengaram, U.J. and Yap, S.P. (2018), "Behavior of fiber-reinforced cementitious composite containing high-volume fly ash at elevated temperatures", *Sadha*, **43**(11), 1-8. <https://doi.org/10.1007/s12046-018-0937-4>
- Mohammed, B.S., Khed, V.C. and Nuruddin, M.F. (2018), "Rubbercrete mixture optimization using response surface methodology", *J. Cleaner Prod.*, **171**, 1605-1621. <https://doi.org/10.1016/j.jclepro.2017.10.102>
- Morsy, M.S., Abbas, H. and Alsayed, S.H. (2012), "Behavior of blended cement mortars containing nano-metakaolin at elevated temperatures", *Constr. Build. Mater.*, **35**, 900-905. <https://doi.org/10.1016/j.conbuildmat.2012.04.099>
- Murray, C.A., Snyder, K.S. and Marion, B.A. (2014), "Characterization of permeable pavement materials based on recycled rubber and chitosan", *Constr. Build. Mater.*, **69**, 221-231. <https://doi.org/10.1016/j.conbuildmat.2014.07.047>
- Nikbin, I.M., Davoodi, M.R., Fallahnejad, H. and Rahimi, S. (2016), "Influence of mineral powder content on the fracture behaviors and ductility of self-compacting concrete", *J. Mater. Civil Eng.*, **28**(3), 04015417. [https://doi.org/10.1061/\(ASCE\)MT.1943-5533.0001404](https://doi.org/10.1061/(ASCE)MT.1943-5533.0001404)
- Rezaifar, O., Hasanzadeh, M. and Gholhaki, M. (2016), "Concrete made with hybrid blends of crumb rubber and metakaolin: Optimization using Response Surface Method", *Constr. Build. Mater.*, **123**, 59-68. <https://doi.org/10.1016/j.conbuildmat.2016.06.047>
- Ritter, A. and Muñoz-Carpena, R. (2013), "Performance evaluation of hydrological models: statistical significance for reducing subjectivity in goodness-of-fit assessments", *J. Hydrol.*, **480**, 33-45. <https://doi.org/10.1016/j.jhydrol.2012.12.004>
- Sahmaran, M. and Li, V.C. (2007), "De-icing salt scaling resistance of mechanically loaded engineered cementitious composites", *Cement Concrete Res.*, **37**, 1035-1046. <https://doi.org/10.1016/j.cemconres.2007.04.001>
- Şahmaran, M., Lachemi, M. and Li, V.C. (2010), "Assessing Mechanical Properties and Microstructure of Fire-Damaged Engineered Cementitious Composites", *ACI Mater.*, **107**(3), 297-304. <https://doi.org/10.14359/51663759>
- Şahmaran, M., Özbay, E., Yücel, H.E., Lachemi, M. and Li, V.C. (2011), "Effect of fly ash and PVA fiber on microstructural damage and residual properties of engineered cementitious composites exposed to high temperatures", *J. Mater. Civil Eng.*, **23**, 1735-1745. <https://doi.org/10.1061/%28ASCE%29MT.1943-5533.0000335>
- Salehi, H. and Mazloom, M. (2018), "Effect of magnetic-field intensity on fracture behaviors of self-compacting lightweight concrete", *Mag. Concrete Res.*, **71**(13), 665-679. <https://doi.org/10.1680/jmacr.17.00418>
- Salehi, H. and Mazloom, M. (2019a), "Opposite effects of ground granulated blast-furnace slag and silica fume on the fracture behavior of self-compacting lightweight concrete", *Constr. Build. Mater.*, **222**, 622-632. <https://doi.org/10.1016/j.conbuildmat.2019.06.183>
- Salehi, H. and Mazloom, M. (2019b), "An experimental investigation on fracture parameters and brittleness of self-compacting lightweight concrete containing magnetic field treated water", *Arch. Civil Mech. Eng.*, **19**, 803-819. <https://doi.org/10.1016/j.acme.2018.10.008>
- Şimşek, B., Uygunođlub, T., Korucua, H.M. and Kocakerim, M.M. (2018), "Analysis of the effects of dioctyl terephthalate obtained from polyethylene terephthalate wastes on concrete mortar: A response

- surface methodology-based desirability function approach application”, *J. Cleaner Prod.*, **170**, 437-445. <https://doi.org/10.1016/j.jclepro.2017.09.176>
- Tyagi, M., Rana, A., Kumari, S. and Jagadevan, S. (2018), “Adsorptive removal of cyanide from coke oven wastewater onto zero-valent iron: Optimization through response surface methodology, isotherm and kinetic studies”, *J. Cleaner Prod.*, **178**, 398-407. <https://doi.org/10.1016/j.jclepro.2018.01.016>
- Wang, Y.C., Zhang, B.J and Hao, S.W. (2016), “Time – dependent brittle creep-relaxation failure in concrete”, *Mag. Concrete Res.*, **68**(13), 692-700. <https://doi.org/10.1680/jmacr.15.00186>
- Yang, E. and Li, V.C. (2010), “Strain-hardening fiber cement optimization and component tailoring by means of a micromechanical model”, *Constr. Build. Mater.*, **24**, 130-139. <https://doi.org/10.1016/j.conbuildmat.2007.05.014>
- Yu, J., Weng, W. and Yu, K. (2014), “Effect of different cooling regimes on the mechanical properties of cementitious composites subjected to high temperatures”. <https://doi.org/10.1155/2014/289213>
- Yu, J., Lin, J., Zhang, Z. and Li, V.C. (2015), “Mechanical performance of ECC with high-volume fly ash after sub-elevated temperatures”, *Constr. Build. Mater.*, **99**, 82-89. <https://doi.org/10.1016/j.conbuildmat.2015.09.002>
- Zhang, Y., Liu, Z. and Yao, L. (2019), “Mechanical properties of high-ductility cementitious composites with methyl silicone oil”, *Mag. Concrete Res.*, **72**(14), 747-756. <https://doi.org/10.1680/jmacr.18.00192>